

General Quantum Bernoulli Factory: Framework Analysis and Experiments

Yong Liu,^{1,*} Jiaqing Jiang,^{2,3,*} Pingyu Zhu,¹ Dongyang Wang,¹ Jiangfang Ding,¹
Xiaogang Qiang,^{1,4} Anqi Huang,¹ Ping Xu,¹ Jialin Zhang,^{2,3} Guojing Tian,^{2,3} Xiang Fu,¹
Mingtang Deng,¹ Chunqing Wu,¹ Xiaoming Sun,^{2,3,†} Xuejun Yang,¹ and Junjie Wu^{1,‡}

¹*Institute for Quantum Information & State Key Laboratory of High Performance Computing,
College of Computer, National University of Defense Technology, Changsha 410073, China*

²*Institute of Computing Technology, Chinese Academy of Sciences, Beijing 100190, China*

³*University of Chinese Academy of Sciences, Beijing 100049, China*

⁴*National Innovation Institute of Defense Technology, AMS, 100071 Beijing, China*

The unremitting pursuit for quantum advantages gives rise to the discovery of a quantum-enhanced randomness processing named quantum Bernoulli factory. In this quantum enhanced process, quantum advantages can be proved through the readily available quantum resources. In this work, we thoroughly study the quantum state evolution within the quantum Bernoulli factory, allowing arbitrary unitary operations or measurements for producing multiparticle states. Theoretically we find a field structure of the constructible states, with which we further provide a framework analysis for the quantum Bernoulli factory, showing that the previous works can be viewed as specific examples within this framework. As a proof of principle, we experimentally demonstrate the quantum Bernoulli factory via an entangled two-photon source along with a reconfigurable photonic logic, and show the quantum advantages through a classically infeasible case by purely quantum operations. These results may stimulate the quantum advantages in simulating wider range of classically infeasible random processes.

I. INTRODUCTION

Quantum computers are trusted to be advanced over the classical machines in the field of information processing, because of the counterintuitive features of quantum mechanics [1–4], especially the quantum superposition and the entanglement [5, 6]. Despite that the current capabilities of quantum computers are confronted with the challenges from their classical competitors [7–9], quantum computing is moving towards the era of “quantum supremacy” [10, 11]. During the pursuit for building practical quantum devices, it’s found that quantum advantages can be proved immediately in a model of randomness processing named quantum Bernoulli factory [3].

Consider the following task: given a biased coin with unknown probability p for head, can we simulate a balanced coin? The solution is that toss this coin twice, and output the result of the second toss if the two outcomes are different, or repeat the toss if they are the same [13]. In this way we obtain a classical Bernoulli factory (CBF) [7, 15, 16] for a balanced coin, i.e. a $f(p)$ -coin with $f(p) = \frac{1}{2}$. This concept can be generalized for an arbitrary constructible function $f(p) : (\mathbb{P} \subseteq [0, 1]) \rightarrow [0, 1]$ that satisfies the following three conditions: (1) it is continuous on its domain; (2) it doesn’t reach 0 or 1 within its domain; (3) it doesn’t approach 0 or 1 exponentially fast near any edge of its domain [2]. For some functions, such as $f(p) = p^2$, it is easy to find such a process.

However, functions violating the conditions are infeasible for the CBF, such as the “Bernoulli doubling” function $f_{\wedge}(p) = 2p, p \in [0, \frac{1}{2}]$ [18].

Significantly, generating $f_{\wedge}(p)$ becomes theoretically feasible on the *quantum Bernoulli factory* (QBF) [3]. The QBF starts from a quantum coin (or *quoin*), which is represented by a state $|\psi_p\rangle = \sqrt{p}|0\rangle + \sqrt{1-p}|1\rangle$ where p is the unknown parameter. By applying unitary operations on $|\psi_p\rangle$ and then measuring the state, classical infeasible coins can be constructed, and with further classical processing on the measured results, strictly more results can be produced in QBF than those can be produced in CBF. The $f_{\wedge}(p)$ -coin can be generated by using single-qubit unitary operations on $|\psi_p\rangle$ and measurements, associated with further classical coin tossing, or can be more efficiently constructed by conducting bell measurement on $|\psi_p\rangle \otimes |\psi_p\rangle$ along with much less classical operations.

These advantages were immediately experimentally demonstrated [4, 5]. However, the proposed QBFs are equipped with quantum processors customized for the Bernoulli doubling function $f_{\wedge}(p) = 2p$. It’s wondering that whether the quantum advantages within the QBF would be further enhanced if the quantum processors support arbitrary operations. In respect of this question, a study remove the restriction of unitary operations, but merely answered what single-qubit quantum states can be constructed from $|\psi_p\rangle$, which is known as the quantum-to-quantum Bernoulli factory [1].

In this work, we provide a thorough study about the processes of quantum state evolution within QBF by generalizing the quantum-to-quantum Bernoulli factory to cases where multi-qubit states are produced, and find a field structure of the constructible multiparticle states, which then allow post-selection when measuring the result states to produce input coins for the following clas-

*These authors contribute equally to this work.

†Electronic address: sunxiaoming@ict.ac.cn

‡Electronic address: junjiewu@nudt.edu.cn

sical processing. We then provide a framework analysis about QBF, so that the previous works can be viewed as specific instances. Our analysis indicates that a multi-qubit quantum processor can provide various enhancement in efficiency and a larger set of quantumly solvable problems. As a proof of principle, we experimentally demonstrate the QBF, and show the quantum advantages through a classically infeasible coin constructed through purely quantum operations.

II. RESULTS

Generalizing quantum-to-quantum Bernoulli factory for producing multi-qubit states. The quantum-to-quantum Bernoulli factory starts from the state $|\psi_p\rangle$, and produce states in the form of $|\psi_o\rangle = k_0(p)|0\rangle + k_1(p)|1\rangle$, where $k_0(p)$ and $k_1(p)$ are functions of p satisfying $|k_0(p)|^2 + |k_1(p)|^2 = 1$. For a single-qubit state, generally we can rewrite it as

$$|h(p)\rangle = c(p) (h(p)|0\rangle + |1\rangle), \quad (1)$$

where $c(p)$ is the coefficient for normalization, and $h(p)$ is a function of p . We say that a state $|h(p)\rangle$ is constructible if it can be transformed from $|\psi_p\rangle$ in finite steps. In each step, we can use unitary operation or measurement, along with some auxiliary qubits. The auxiliary qubits can be either constructible states, or some constant single-qubit states in which the amplitudes are constant complex numbers. It has been proved that $|h(p)\rangle$ is constructible if and only if $h(p)$ belongs to the field \mathbb{M} generated from $\sqrt{\frac{p}{1-p}}$ and the complex field (see supplementary for formula definition).

Now we remove the restriction on the quantity of qubits contained in the result state. That is to produce an n -qubit state

$$|K(p)\rangle = \sum_{i=0}^{2^n-1} k_i(p)|i\rangle, \quad (2)$$

from several copies of $|\psi_p\rangle$ in finite steps, where $n \geq 1$ and $k_i(p)$ are functions of p , satisfying $\sum_{i=0}^{2^n-1} |k_i(p)|^2 = 1$. We denote all the constructible states by the notion of *Bernoulli states*. For general cases, $|K(p)\rangle$ may not be the direct product of n single-qubit states because of the entanglement, and has to be considered as a whole. Similarly, we can rewrite the n -qubit Bernoulli state as

$$|K(p)\rangle = c(p) \left(\sum_{i=0}^{2^n-2} h_i(p)|i\rangle + |2^n-1\rangle \right), \quad (3)$$

where $h_i(p) = k_i(p)/k_{2^n-1}(p)$, and $c(p)$ is used for normalization. In the following, we will ignore the normalization coefficient for simplicity. It is obvious that for arbitrary constructible states, each $h_i(p)$ belongs to the same set, because any two amplitudes can be switched

under specific unitary operations. Let \mathbb{S} be the set of $h_i(p)$ from all constructible $|K(p)\rangle$. Our result is the following theorem.

Theorem. An n -qubit state $|K(p)\rangle = \sum_{i=0}^{2^n-2} h_i(p)|i\rangle + |2^n-1\rangle$ is constructible if and only if each $h_i(p)$ belongs to the field \mathbb{M} .

Note that \mathbb{M} is the same field which is used to characterize the constructible states in single-qubit cases. To construct arbitrary states, it only requires a small set of basic unitary operations. The proof and the approach to construct arbitrary Bernoulli states are placed in the supplementary methods [22].

The framework of quantum Bernoulli factory. A QBF mainly contains two key phases, the state evolution and measurement on a quantum processor, together with the following classical processing. If no quantum operations are supported, the process is a CBF, as shown in Fig. 1(a). A quantum processor can enhance the process in many aspects. To analyze the enhancement, we divide the QBF into three types, as shown in Fig. 1(b).

(1) The first type is the QBF that supports only single qubit operations for quantum state evolution. Specifically, the only type of unitary used is

$$U_a = \begin{bmatrix} \sqrt{a} & \sqrt{1-a} \\ \sqrt{1-a} & -\sqrt{a} \end{bmatrix}, \quad (4)$$

where a is a real number, and the functions constructed from the evolution result state is in a fixed format of $f_a(p) = \left| \sqrt{a(1-p)} - \sqrt{p(1-a)} \right|^2$, which form a set denoted by \mathbb{Q}_1^1 . In this notation, the '1's in the superscript and subscript respectively represent that the output states and the unitary operations are restricted in 1 qubit. For $a \in (0, 1)$, $f_a(p)$ is not classically constructible because $f_a(p)$ reaches 0 when $p = a$. Associated with the further classical processing, it can reach a result set (denoted by $\mathbb{Q}_1^1\mathbb{C}$) that is strictly larger than the purely classical processes [3].

(2) For the second type, the QBF is enhanced by allowing arbitrary quantum operations for state evolution, and constructing a single-qubit state $|\psi_o\rangle = k_0(p)|0\rangle + k_1(p)|1\rangle$ to generate $|k_0(p)|^2$ -coins for further classical processing. During the process, the quantumly constructed coins, i.e. the $|k_0(p)|^2$ -coins, form a set denoted by \mathbb{Q}^1 , and finally the classical processing can reach a set labelled as $\mathbb{Q}^1\mathbb{C}$. However, it has been proved that $\mathbb{Q}^1 \subsetneq \mathbb{Q}_1^1\mathbb{C}$ [1], which indicates that $\mathbb{Q}_1^1\mathbb{C} = \mathbb{Q}^1\mathbb{C}$ (see supplementary for details). The enhancement on the quantum processor mainly accelerate the construction for some specific functions.

(3) Finally, the quantum processor is further enhanced by allowing arbitrary quantum operations and generating an n -qubit Bernoulli state (see equation (3)). Then we can apply joint measurement on this state, and apply post-selection to construct functions in the form of

$$q(p) = \frac{\sum_{j \in \mathbb{H}} |h_j(p)|^2}{\sum_{i \in \mathbb{B}} |h_i(p)|^2}, \quad (5)$$

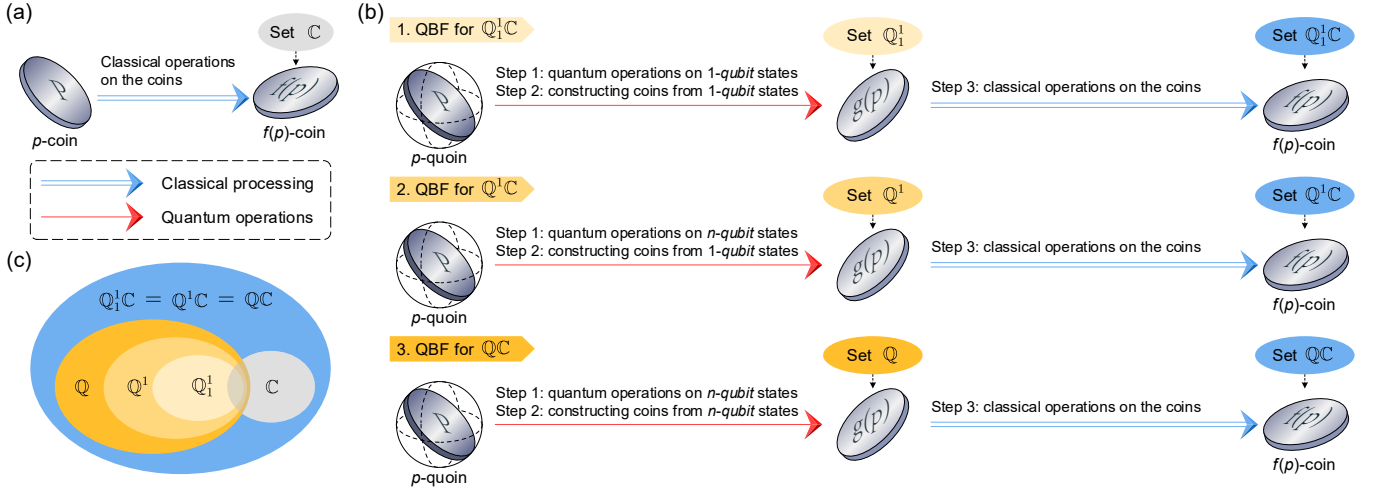


FIG. 1: **The framework analysis of quantum Bernoulli factory.** (a) the classical Bernoulli factory (CBF), which can construct functions in set \mathbb{C} ; (b) the quantum Bernoulli factories with different quantum processors. They first evolve the p -quoins ($|\psi_p\rangle$) with supported operations, and transform the result states into classical probabilities through the measurement which respectively constitute constructible sets denoted by Q_1^1 , Q^1 or Q , where the superscript and subscript respectively represent that the constructible states and the unitary operations in the quantum processor are restricted in 1 qubit. The whole QBF processes can construct coins from set Q_1^1C , Q^1C and QC respectively. (c) The relationship between the constructible sets. We find the equality among the QC sets.

where \mathbb{B} is the set of bases remained within the post selection, and $\mathbb{H} \subseteq \mathbb{B}$ is the set of bases chosen for a head output. The post-selection along with the multiparticle states allow a wider range of quantumly constructible coins, which forms the set denoted as Q , and the complete set after classical processing is denoted as QC . The proposed experiment in ref. [5] using Bell measurement for $4p(1-p)$ -coin is an example of this strategy, showing the advantage of post-selection in efficiency. We further provide the protocols for $g(p)$ -coin on QBFs of different types in supplementary methods for clearer comparison. There are also some interesting results about the classical coins generated. We can make some breakpoints of the function $k_c(p)$, that is for some values of p , $h_i(p) = 0$ for every $i \in \mathbb{B}$. Nevertheless, these singularities can still be handled, resulting in that the functions constructed are still within the range of Q_1^1C , which further indicates the equality between Q_1^1C and QC [22]. In summary, the relationship of the constructible sets are shown in Fig. 1(c).

Experimental demonstration. The classical coin-flips can be easily realized on a personal computer, therefore the experimental hardness concentrates on the implementation of the quantum processor. Without losing generality, reaching all possible single-qubit Bernoulli states requires a set of basic operations for manipulating the relative amplitudes of states, including multiplicative inverse, multiplication and addition [1, 22], which is used for expanding the field of Bernoulli states corresponding to \mathbb{M} (see Fig. 2(a)), and can be generalized for constructing arbitrary Bernoulli states.

As a proof-of-principle experiment, we design, simplify and demonstrate the circuits for the two-qubit basic operations, see Fig. 2(b-d). For our experimental case, the inverse operation can be easily implemented by using a

Pauli X gate. We focus on the realization of the multiply and add operations. The multiply operation can be implemented with two qubits and a C-NOT gate. The simplified circuit for add operation uses a C- M_0X gate, which is implemented by adding control to a group of gate operations [23, 24]

$$C\text{-}M_0X = M_0 \otimes I + M_1 \otimes (M_0 \cdot X), \quad (6)$$

where $M_0(M_1)$ is the projection operator to $|0\rangle(|1\rangle)$.

We built a configurable two-qubit photonic processor, as shown in Fig. 2(e). By configuring the photonic logic, we can produce states $|h_1 \cdot h_2\rangle$ and $|h_1 + h_2\rangle$ for multiply operation and add operation respectively. We take some typical states or random states as input, then measure the fidelities of the output states. The results are shown in Fig. 3. The average fidelity of the states generated by multiply operations and add operations are 95.58% and 96.52% respectively.

Within the photonic logic, the C-NOT gate is the key component of the circuits, and has to be implemented with high quality. We evaluate the fidelity of the implemented C-NOT gate using the method proposed in [6]. The process fidelity of the C-NOT gate can be evaluated through the measurement of two truth tables in complementary bases. We choose $|H\rangle/|V\rangle$ basis and $|D\rangle/|A\rangle$ basis for fidelity evaluation, and bound the process fidelity (F_P) through

$$F_{HV} + F_{DA} - 1 \leq F_P \leq \min(F_{HV}, F_{DA}), \quad (7)$$

where $F_{HV}(F_{DA})$ is the fidelity of the truth table measured in $|H\rangle/|V\rangle$ ($|D\rangle/|A\rangle$) basis. The results of the fidelities of the two truth tables are shown in Fig. 4, then we can evaluate the process fidelity of the C-NOT gate as

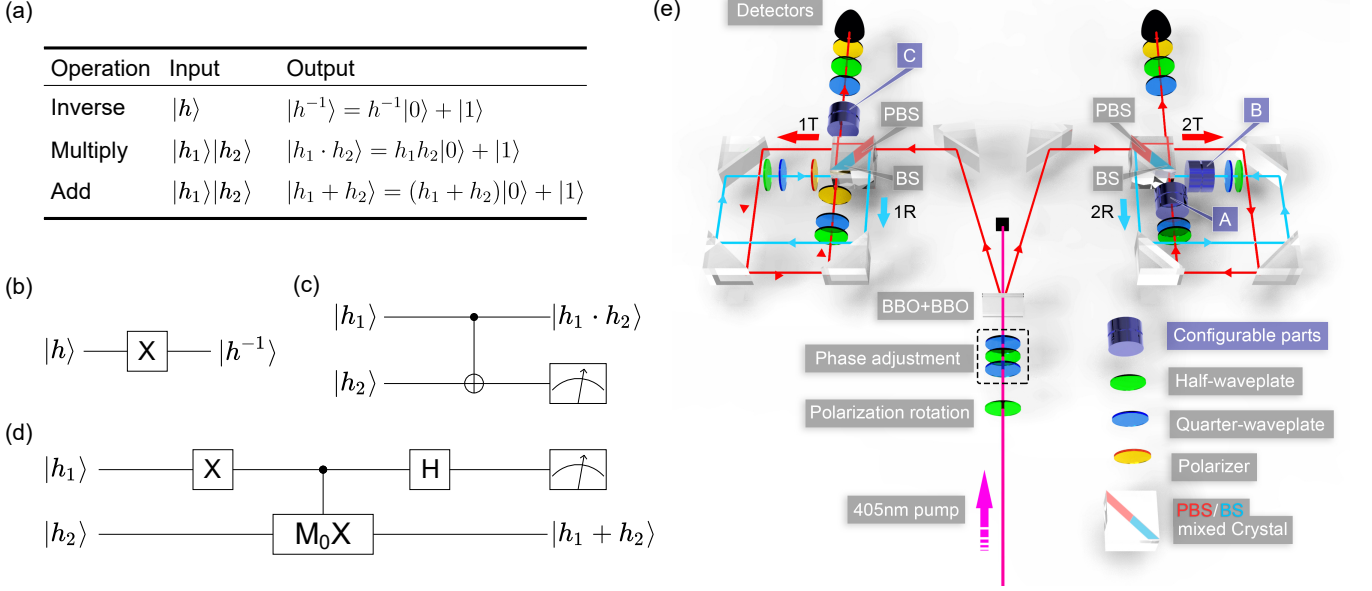


FIG. 2: **The experimental proposal.** (a) The set of basic operations for expanding the field of single-qubit Bernoulli states. (b-d) The circuits for the basic operations. (b) Circuits for the inverse operation; (c) Circuits for the multiply operation. It requires two qubits and a C-NOT gate on them; (d) Circuits for the add operation. The control- M_0X gate is obtained through equation (6). (e) The experimental principle. The main part of the experimental setup is a configurable two-qubit gate implemented with two displaced Sagnac interferometers. The whole process is activated by a pair of entanglement photons produced through type-I spontaneous parametric down conversion (SPDC). A, B and C are configurable parts, representing different combinations of optical elements for different operations.

$91.40\% \leq F_P \leq 94.16\%$. Our results offer a tight bound for the fidelity of this C-NOT gate.

Experimental quantum advantage. A powerful quantum processor can directly construct various coins

with better efficiency. Here we take an example of a $f_c(p)$ -coin, where $f_c(p) = 1 - \frac{1}{1+(2p-1)^2}$, and experimentally demonstrate this case. This function is classically infeasible because $f_c(\frac{1}{2}) = 0$, while it can be constructed by directly measuring the Bernoulli state

$$|f_q(p)\rangle = (2p-1)|0\rangle + |1\rangle, \quad (8)$$

which can be constructed without any classical processing. We design the circuit for this state by the basic operations, and then simplify it to suit our photonic logic, as shown in Fig. 5(a). The key component is also a C-NOT gate, but the part C is set to be Hadamard gate followed by a X gate.

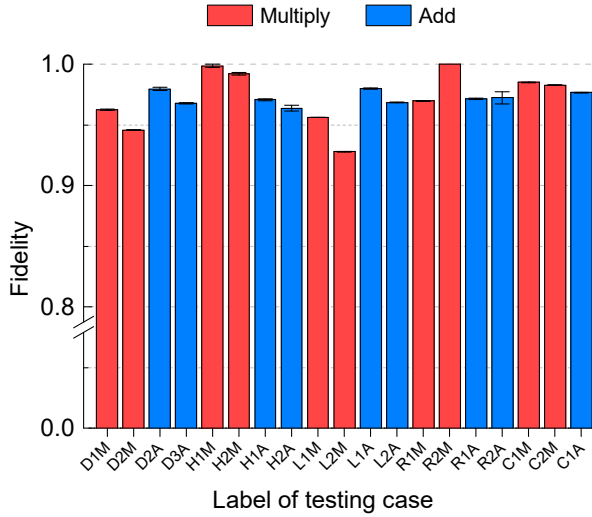


FIG. 3: **Fidelity of the multiply and add operations.** The x-tick is the label of the test case, the corresponding detailed data can be found in supplementary information. The initial letter of the label represents the type of the input states, where “D” refers to $|D\rangle/|A\rangle$ basis, “H” refers to $|H\rangle/|V\rangle$ basis, “L” refers to $|L\rangle/|R\rangle$ basis. “R” (“C”) refers to random states with the parameters chosen to be real (complex) random numbers. The error bars stand for one standard deviation.

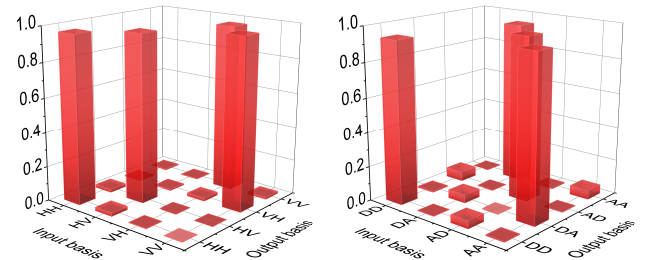


FIG. 4: **The results of truth tables of the C-NOT gate.** We choose $\{|HH\rangle, |HV\rangle, |VH\rangle, |VV\rangle\}$ and $\{|DD\rangle, |DA\rangle, |AD\rangle, |AA\rangle\}$ as the bases for fidelity evaluation. Fidelities of the truth tables are $97.24 \pm 0.65\%$ ($|H\rangle/|V\rangle$) and $94.16 \pm 0.59\%$ ($|D\rangle/|A\rangle$) respectively. The truth tables are obtained through coincidence counts, with each high column being around 2,000.

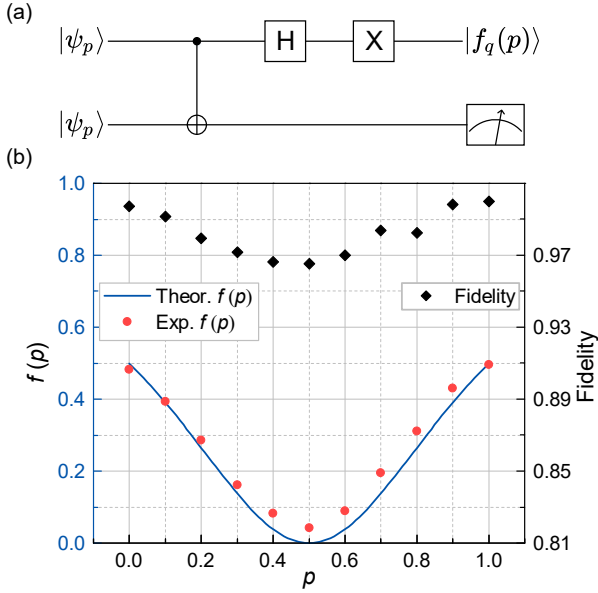


FIG. 5: **The circuit for the example coin and the results.** (a) Circuits for generating $f_q(p)$ -quoin. (b) Experimental results of generating $f_c(p)$ -coin. The black solid rhombuses are the fidelities of the states corresponding to different value of p , where the error bars are too small to be visible. The probabilities (red circles) are obtained through coincidence counts with the total counts accumulated for about 1 minute, and the photon-pair counts recorded ranges from around 400 to about 1,000 according to the different value of p .

We measured the fidelity of the outcome states, and then get the success probability of the output coins by measuring the output state in σ_z basis. The average fidelity of the states is 98.23%, and the results agree the theoretical values well, as shown in Fig. 5(b). The success probability of the construction is $\text{Pr}_c = ((2p - 1)^2 + 1) / 16$, which reaches the minimum value of $1/16$ when $p = 0.5$. Owing to the post-selection and photon loss, we need averagely less than 100 quoins to construct this coin for $p = 0.5$. Because of the experimental imperfection, the experimental value at the violation point is 0.042, which corresponds to a truncation of

$$f_{ct}(p) = \max\left(1 - \frac{1}{1 + (2p - 1)^2}, \varepsilon\right), \quad (9)$$

where $\varepsilon = 0.042$. This truncation offers possibility for classically constructing $f_{ct}(p)$. Here we provide a classical protocol for constructing $f_{ct}(p)$ -coin. We noticed that $(2p - 1)^2 = 1 - 4p(1 - p)$. Therefore the elementary step of generating the $(2p - 1)^2$ -coin can follow the same procedure of constructing $g(p) = 4p(1 - p)$ with a corresponding truncation error of $\varepsilon_g = 0.044$, which requires about 2.285×10^4 classical coins when $p = 0.5$ [4, 7, 22]. Then $f_{ct}(p)$ can be constructed through generating $k(p) = l(p)/(1 + l(p))$, where $l(p) = (2p - 1)^2$. In this procedure, the average consumption of $l(p)$ coins is $2/(1 - l(p))^2 = 2.190$. In summary, the full procedure

for constructing $f_{ct}(p)$ coin requires 5.003×10^4 classical coins. Note that this classical protocol may not be the optimal one, but is enough for showing the quantum advantage.

III. DISCUSSION

In this work, we thoroughly answer the question about what states can be implemented from $|\psi_p\rangle$, regardless of the limit on the quantity of qubits. A more powerful quantum processor within a QBF can benefit in three aspects. (1) It can greatly enhance the construction efficiency; (2) It can reduce the resource consumption by orders of magnitude; (3) The quantum processor itself can directly generate classical coins from wider range. These advantages provide better stimulations with quantum advantages in the randomness processing. Besides, as we find that the non-unitary operations may bring in more speedup, as it was reflected by the simplified circuits of the add operation in the experiment, the quantum Bernoulli factory may still be further enhanced if non-unitary operations are allowed.

We experimentally demonstrate the quantum Bernoulli factory and show the quantum advantages in the efficiency and the resource consumption. These advantages are based on the theoretical priority of the quantum mechanism that the information encoded in the states can reach the complex field before being transferred into classical information. The classical protocol we provided is not optimal, but is enough for showing the quantum advantages. However, though the benefits of multiparticle operations are significant, they do bring in more experimental hardness. Our experimental setup is more complicated than previous experiments, and therefore is more sensitive to noise or subtle imperfect settings of the optical elements, requiring comprehensive balance between the processing efficiency, complexity of implementation and the fidelity of the result.

IV. METHODS

Experimental setup. In the setup (see Fig. 2(e)), entangled photons are generated through the type-I SPDC process by focusing a diagonally polarized continuous-wave laser beam with central wavelength of 405nm onto two orthogonal BBO crystals, generating state $|\psi_0\rangle = (|00\rangle + |11\rangle)/\sqrt{2}$, where $|0\rangle$ and $|1\rangle$ represent the horizontal polarization state and vertical polarization state respectively. Then the entangled photons are injected into two Sagnac structures. Within the Sagnac loops, the entangled photons are converted to be spatially entangled through the PBS part (the red reflecting surface) of the PBS/BS mixed crystal. In each spatial path, a half-waveplate and a quarter-waveplate are used for en-

coding the input state

$$|\psi_{in}\rangle = \frac{1}{\sqrt{2}}(|h_1\rangle_{1T}|h_2\rangle_{2T} + |h_1\rangle_{1R}|h_2\rangle_{2R}), \quad (10)$$

where the h_1 and h_2 are parameters of the input Bernoulli states. The four spacial modes pass through different optical elements. The polarizers in the “1T” and “1R” paths are fixed to be horizontal and vertical respectively. By placing different combinations of optical elements in the configurable parts labeled as A and B in the logic, we can implement different two-qubit operations. After being mixed in the BS part of the mixed crystal (the reflecting surface marked blue), and further operated by the configurable parts C , the state becomes

$$|\psi_o\rangle = (I \otimes C)(M_0 \otimes A + M_1 \otimes B)|h_1\rangle|h_2\rangle. \quad (11)$$

The state identification is done through a polarizer associated with a quarter-waveplate and a half-waveplate, and another polarizer is used for post-selection. At last, photons are filtered with two $3nm$ band filters.

For the multiply operation, the photonic logic is configured as a C-NOT gate. Specifically, the parts A and C are configured as identity, part B is configured as a X gate. We then measure the second qubit. If we get $|0\rangle$, the remaining qubit collapsed to $|\psi_{\times}\rangle = (h_1h_2|0\rangle + |1\rangle)$. For the add operation, we configure A as identity, B as $X \cdot M_0$, and C as a Hadamard gate. The first X gate applied on the first qubit is merged into the state initialization by preparing the initial state to be $|h_1^{-1}\rangle|h_2\rangle$. If we get $|0\rangle$ when measuring the first qubit, the remaining qubit will collapse to $|\psi_{+}\rangle = (h_1 + h_2)|0\rangle + |1\rangle$.

-
- [1] Michael A. Nielsen and Isaac Chuang. Quantum computation and quantum information. *American Journal of Physics*, 70(5):558–559, 2002.
 - [2] Charles H. Bennett and Gilles Brassard. Quantum cryptography: Public key distribution and coin tossing. *Theoretical Computer Science*, 560:7 – 11, 2014. Theoretical Aspects of Quantum Cryptography - celebrating 30 years of BB84.
 - [3] Nicolas Gisin and Rob Thew. Quantum communication. *Nature Photonics*, 1:165 EP –, Mar 2007. Review Article.
 - [4] Artur K. Ekert. Quantum cryptography based on bell’s theorem. *Phys. Rev. Lett.*, 67:661–663, Aug 1991.
 - [5] Lov K. Grover. A fast quantum mechanical algorithm for database search. In *Proceedings of the Twenty-eighth Annual ACM Symposium on Theory of Computing*, STOC ’96, pages 212–219, New York, NY, USA, 1996. ACM.
 - [6] P. W. Shor. Algorithms for quantum computation: discrete logarithms and factoring. In *Proceedings 35th Annual Symposium on Foundations of Computer Science*, pages 124–134, Nov 1994.
 - [7] Xiangke Liao, Liquan Xiao, Canqun Yang, and Yutong Lu. Milkyway-2 supercomputer: system and application. *Frontiers of Computer Science*, 8(3):345–356, Jun 2014.
 - [8] Junjie Wu, Yong Liu, Baida Zhang, Xianmin Jin, Yang Wang, Huiquan Wang, and Xuejun Yang. A benchmark test of boson sampling on Tianhe-2 supercomputer. *National Science Review*, 5(5):715–720, 07 2018.
 - [9] Chu Guo, Yong Liu, Min Xiong, Shichuan Xue, Xiang Fu, Anqi Huang, Xiaogang Qiang, Ping Xu, Junhua Liu, Shenggen Zheng, He-Liang Huang, Mingtang Deng, Dario Poletti, Wan-Su Bao, and Junjie Wu. General-purpose quantum circuit simulator with projected entangled-pair states and the quantum supremacy frontier. *Phys. Rev. Lett.*, 123:190501, Nov 2019.
 - [10] John Preskill. Quantum computing and the entanglement frontier. *arXiv*, (1203.5813), 2012.
 - [11] Frank Arute, Kunal Arya, Ryan Babbush, Dave Bacon, Joseph C. Bardin, Rami Barends, Rupak Biswas, Sergio Boixo, Fernando G. S. L. Brandao, David A. Buell, Brian Burkett, Yu Chen, Zijun Chen, Ben Chiaro, Roberto Collins, William Courtney, Andrew Dunsworth, Edward Farhi, Brooks Foxen, Austin Fowler, Craig Gidney, Marissa Giustina, Rob Graff, Keith Guerin, Steve Habegger, Matthew P. Harrigan, Michael J. Hartmann, Alan Ho, Markus Hoffmann, Trent Huang, Travis S. Humble, Sergei V. Isakov, Evan Jeffrey, Zhang Jiang, Dvir Kafri, Kostyantyn Kechedzhi, Julian Kelly, Paul V. Klimov, Sergey Knysh, Alexander Korotkov, Fedor Kostritsa, David Landhuis, Mike Lindmark, Erik Lucero, Dmitry Lyakh, Salvatore Mandrà, Jarrod R. McClean, Matthew McEwen, Anthony Megrant, Xiao Mi, Kristel Michielsen, Masoud Mohseni, Josh Mutus, Ofer Naaman, Matthew Neeley, Charles Neill, Murphy Yuezhen Niu, Eric Ostby, Andre Petukhov, John C. Platt, Chris Quintana, Eleanor G. Rieffel, Pedram Roushan, Nicholas C. Rubin, Daniel Sank, Kevin J. Satzinger, Vadim Smelyanskiy, Kevin J. Sung, Matthew D. Trevithick, Amit Vainsencher, Benjamin Villalonga, Theodore White, Z. Jamie Yao, Ping Yeh, Adam Zalcman, Hartmut Neven, and John M. Martinis. Quantum supremacy using a programmable superconducting processor. *Nature*, 574(7779):505–510, 2019.
 - [12] Howard Dale, David Jennings, and Terry Rudolph. Provable quantum advantage in randomness processing. *Nature Communications*, 6:8203 EP –, Sep 2015. Article.
 - [13] J. von Neumann. Various techniques used in connection with random digits. *Appl. Math. Ser.*, 12, 1951.
 - [14] Șerban Nacu and Yuval Peres. Fast simulation of new coins from old. *Ann. Appl. Probab.*, 15(1A):93–115, 02 2005.
 - [15] Krzysztof Łatuszyński, Ioannis Kosmidis, Omiros Paspaliopoulos, and Gareth O. Roberts. Simulating events of unknown probabilities via reverse time martingales. *Random Structures & Algorithms*, 38(4):441–452, 2011.
 - [16] A. C. Thomas and Jose H. Blanchet. A practical implementation of the bernoulli factory. *arXiv*, (1106.2508), 2011.
 - [17] M. S. Keane and George L. O’Brien. A bernoulli factory. *ACM Trans. Model. Comput. Simul.*, 4(2):213–219, April 1994.
 - [18] Mark Huber. Nearly optimal bernoulli factories for linear functions. *Combinatorics, Probability and Computing*, 25(4):577–591, 2016.

- [19] Xiao Yuan, Ke Liu, Yuan Xu, Weiting Wang, Yuwei Ma, Fang Zhang, Zhaopeng Yan, R. Vijay, Luyan Sun, and Xiongfeng Ma. Experimental quantum randomness processing using superconducting qubits. *Phys. Rev. Lett.*, 117:010502, Jun 2016.
- [20] Raj B. Patel, Terry Rudolph, and Geoff J. Pryde. An experimental quantum bernoulli factory. *Science Advances*, 5(1), 2019.
- [21] Jiaqing Jiang, Jialin Zhang, and Xiaoming Sun. Quantum-to-quantum bernoulli factory problem. *Phys. Rev. A*, 97:032303, Mar 2018.
- [22] See supplementary information for details.
- [23] Xiao-Qi Zhou, Timothy C. Ralph, Pruet Kalasuwan, Mian Zhang, Alberto Peruzzo, Benjamin P. Lanyon, and Jeremy L. O’Brien. Adding control to arbitrary unknown quantum operations. *Nature Communications*, 2:413 EP –, Aug 2011. Article.
- [24] Xiaogang Qiang, Thomas Loke, Ashley Montanaro, Kanin Aungskunsiri, Xiaoqi Zhou, Jeremy L. O’Brien, Jingbo B. Wang, and Jonathan C. F. Matthews. Efficient quantum walk on a quantum processor. *Nature Communications*, 7:11511 EP –, May 2016. Article.
- [25] Holger F. Hofmann. Complementary classical fidelities as an efficient criterion for the evaluation of experimentally realized quantum operations. *Phys. Rev. Lett.*, 94:160504, Apr 2005.

V. ACKNOWLEDGMENTS

We gratefully appreciate the kindly support from China Great wall Technology in Changsha. We also appreciate the helpful discussion with other members of QUANTA team. J. W. acknowledges the support from National Natural Science Foundation of China under Grants No. 61632021. P. X. acknowledges the support from National Natural Science Foundation of China under Grants No. 11621091 and 11690031. X. Q. acknowledges the support from National Natural Science Foundation of China under Grants No. 11804389.

Supplementary Materials

General Quantum Bernoulli Factory: Framework Analysis and Experiments

I. SET REFERENCE

In our paper, there appear many different sets. In this section, we give the formal definitions of the sets in this manuscript.

- Set \mathbb{M}

This set is the field generated from $\sqrt{\frac{p}{1-p}}$ and the complex field, where p is a unknown parameter. Specifically,

$$\mathbb{M} = \left\{ \frac{g_1(p)}{g_2(p)} \sqrt{\frac{p}{1-p}} + \frac{g_3(p)}{g_4(p)} \right\} \quad (\text{S1})$$

where $g_i(p)$ are polynomials of p with complex coefficients [S1].

- Set \mathbb{S}

This set is used to describe the range of Bernoulli states. Specifically, \mathbb{S} is the set of relative amplitudes of the constructible states.

- Set \mathbb{C}

This set contains all constructible functions of classical Bernoulli factory. The characterization of this set can be described by the three conditions in the main text or [S2].

- Set \mathbb{Q}_1^1

It is the set of classical functions constructed by the quantum processor that evolves $|\psi_p\rangle$ using a specific type of unitary (equation (4) in main text), and therefore this set can be written as

$$\mathbb{Q}_1^1 = \{f_a(p) | a \in (0, 1)\}. \quad (\text{S2})$$

where $f_a(p) = \left| \sqrt{a(1-p)} - \sqrt{p(1-a)} \right|^2$.

- Set \mathbb{Q}^1

This set is the constructible functions by firstly using the quantum processor embedded within the type-2 QBF to construct a single-qubit Bernoulli state with arbitrary finite operations, and then measure the single-qubit state to obtain a classical result. Specifically,

$$\mathbb{Q}^1 = \left\{ |k_0(p)|^2 \left| |\psi_o\rangle = k_0(p)|0\rangle + k_1(p)|1\rangle \text{ is a Bernoulli state, i.e., } \frac{k_0(p)}{k_1(p)} \in \mathbb{M} \right\}. \quad (\text{S3})$$

- Set \mathbb{Q}

This set is the constructible functions by the quantum processor of type-3 QBF. This is the general case for set \mathbb{Q}^1 where the state generated are free of restrictions on the number of qubits. Specifically, we generate an n -qubit Bernoulli state $|K(p)\rangle = c(p) \left(\sum_{i=0}^{2^n-2} h_i(p)|i\rangle + |2^n-1\rangle \right)$, and obtain a classical function in set

$$\mathbb{Q} = \left\{ \frac{\sum_{j \in \mathbb{H}} |h_j(p)|^2}{\sum_{i \in \mathbb{B}} |h_i(p)|^2} \left| h_i(p) \in \mathbb{M} \right\} \quad (\text{S4})$$

where $h_i(p)$ are the relative amplitudes of a Bernoulli state, \mathbb{B} is the set of bases chosen in the measurement, and $\mathbb{H} \subseteq \mathbb{B}$ is the set of bases chosen for a head output.

- Set $\mathbb{Q}_1^1 \mathbb{C}$

This set is the constructible functions of type-1 QBF obtained by feeding functions in \mathbb{Q}_1^1 into the classical processing. The characterization of this set is analyzed in [S3].

- Set $\mathbb{Q}^1\mathbb{C}$

This set contains the constructible functions of type-2 QBF, obtained by feeding functions in \mathbb{Q}^1 into the classical processing. We find that this set is equal to $\mathbb{Q}_1^1\mathbb{C}$.

- Set $\mathbb{Q}\mathbb{C}$

This set contains the constructible functions of type-3 QBF, obtained by feeding functions in \mathbb{Q} into the classical processing. We find that this set is equal to $\mathbb{Q}_1^1\mathbb{C}$.

II. PROOF OF THE MAIN THEOREM

Proof. Here we prove $\mathbb{S} = \mathbb{M}$. For simplicity, we write the state in the form of equation (3) in the main text, and omit the normalization coefficient $c(p)$.

- *Necessity:* the necessity ($\mathbb{S} \subseteq \mathbb{M}$) can be easily obtained from the following statement:

Statement [S1]. For any constructible $|\phi\rangle = \sum_j s_j(p)|j\rangle$, the ratio of arbitrary two amplitudes of $|\phi\rangle$ belongs to \mathbb{M} .

- *Sufficiency:* suppose we have implemented a state $|K(p)\rangle = \sum_{i=0}^{2^n-2} h_i(p)|i\rangle + |2^n-1\rangle$, and another single-qubit state $|L(p)\rangle = l(p)|0\rangle + |1\rangle$ where $h_i(p) \in \mathbb{S}$, ($i = 1, 2, \dots, 2^n-2$) and $l(p) \in \mathbb{S}$. Without loss of generality, we show that the relative amplitude of $|0\rangle$ in $|K(p)\rangle$ can be manipulated without changing other relative amplitudes. The other relative amplitudes can be manipulated in the similar way. The set that $h_0(p)$ belongs to is closed under addition and multiply, and containing multiplicative inverse for each element. Thus the set \mathbb{S} is a field which contains element $\sqrt{\frac{p}{1-p}}$ and complex field. In other words, $\mathbb{S} = \mathbb{M}$. The details are shown as below.

- *Inverse:* because $h_0(p) \in \mathbb{S}$, we can implement a single-qubit state $|h_0(p)\rangle = c_0(p)(h_0(p)|0\rangle + |1\rangle)$ according to the theorem of ref. [S1]. Switch the amplitudes of $|0\rangle|0\rangle^{\otimes n}$ and $|1\rangle|2^n-1\rangle$ of $|h_0(p)\rangle|K(p)\rangle$, and then measure the first qubit. If we get $|0\rangle$, the rest qubits will collapse to

$$|K_{h_0^{-1}}(p)\rangle = \frac{1}{h_0(p)}|0\rangle + \sum_{i=1}^{2^n-2} h_i(p)|i\rangle + |2^n-1\rangle. \quad (\text{S5})$$

So $\frac{1}{h_0(p)} \in \mathbb{S}$.

- *Multiply:* apply an $(n+1)$ -qubit unitary operation to switch the amplitudes of $|0\rangle|0\rangle^{\otimes n}$ and $|1\rangle|0\rangle^{\otimes n}$ of $|L(p)\rangle|K(p)\rangle$, and measure the first qubit. If we get $|1\rangle$, the remaining qubits will collapse to

$$|K_{M_0}(p)\rangle = h_0(p)l(p)|0\rangle + \sum_{i=1}^{2^n-2} h_i(p)|i\rangle + |2^n-1\rangle. \quad (\text{S6})$$

Thus $h_0(p)l(p) \in \mathbb{S}$.

- *Add:* It requires an specific $2^{n+1} \times 2^{n+1}$ unitary B_n . This unitary looks like an eye matrix, with part of its diagonal similar to a Hadamard matrix

$$B_n = \begin{bmatrix} 1 & & & & & & \\ & \ddots & & & & & \\ & & \ddots & & & & \\ & & & \ddots & & & \\ & & & & \frac{1}{\sqrt{2}} & \cdots & -\frac{1}{\sqrt{2}} \\ & & & & \vdots & & \vdots \\ & & & & \frac{1}{\sqrt{2}} & \cdots & \frac{1}{\sqrt{2}} \\ & & & & & \ddots & \\ & & & & & & 1 \end{bmatrix} \quad (\text{S7})$$

The up left $\frac{1}{\sqrt{2}}$ appears at the 2^n th diagonal position, and the bottom right $\frac{1}{\sqrt{2}}$ is in the $(2^n + (k+1))$ th position, where $|k\rangle$ is the basis to conduct the add operation. Without loss of generality, we are going to manipulate the relative amplitude $h_0(p)$ with $k = 0$.

Then we apply B on $|L(p)\rangle|K(p)\rangle$, and measure the first qubit. If we get $|1\rangle$, the state will collapse to

$$|K_{A_0}(p)\rangle = \frac{h_0(p) + l(p)}{\sqrt{2}}|0\rangle + \sum_{i=1}^{2^n-2} h_i(p)|i\rangle + |2^n-1\rangle. \quad (\text{S8})$$

Then multiply $|K_{A_0}\rangle$ with a single-qubit constant state $|\psi_a\rangle = \sqrt{2}|0\rangle + |1\rangle$ on basis $|0\rangle$ of $|K_{A_0}(p)\rangle$, we can obtain $h_0(p) + l(p) \in \mathbb{S}$.

Therefore, \mathbb{S} is a field. We initially have access to $|p\rangle$ and arbitrary constant qubits, so the generator of \mathbb{S} contains $\sqrt{\frac{p}{1-p}}$ and the complex field. Then we conclude $\mathbb{M} \subseteq \mathbb{S}$. Combining the necessity and sufficiency, we complete our proof. ■

By using the operations, we know that each amplitude can be manipulated without changing other amplitudes, i.e. each amplitude can be manipulated independently. To apply the basic operations on different amplitudes, one can just slightly modify the auxiliary states and unitary matrix used, and follow the same procedure. As a special case, the unitary of the basic operations for single-qubit cases can be referred from [S1].

III. ALGORITHM FOR GENERATING ARBITRARY CONSTRUCTIBLE n -QUBIT STATES

If $n = 1$, i.e. we are going to construct a single-qubit Bernoulli factory, we can construct it following the procedure in ref. [S1].

If $n > 1$, our method starts from a constant balanced n -qubit state (not necessarily normalized)

$$|\Psi\rangle = \sum_{i=0}^{2^n-1} |i\rangle. \quad (\text{S9})$$

For $|F_n(p)\rangle = \sum_{i=0}^{2^n-2} f_i(p)|i\rangle + |2^n-1\rangle$ where $f_i(p) \in \mathbb{M}$, we can firstly generate a series of single-qubit states

$$|f_i(p)\rangle = f_i(p)|0\rangle + |1\rangle, \quad (i = 0, 1, \dots, 2^n-1) \quad (\text{S10})$$

and then use the multiply operation to multiply $|f_i(p)\rangle$ with $|\Psi\rangle$ on the corresponding basis one by one.

IV. PROOF OF $\mathbb{Q} \subseteq \mathbb{Q}_1^1\mathbb{C}$

Recall that $\mathbb{Q}_1^1\mathbb{C}$ is the final constructible set of type-1 QBF, and \mathbb{Q} is the set of classical coins that can be generated by measuring a Bernoulli state that contains no less than one qubit.

Definition [S3]. A function $f(p) : [0, 1] \rightarrow [0, 1]$ is simple and poly-bounded (SPB) if and only if it satisfies

- (1) f is continuous.
- (2) Both $Z = z_i : f(z_i) = 0$ and $W = w_i : f(w_i) = 1$ are finite sets.
- (3) $\forall z \in Z$, there exist constants $c, \delta > 0$ and integer $k < \infty$ such that

$$c(p - z)^{2k} \leq f(p), \forall p \in [z - \delta, z + \delta]. \quad (\text{S11})$$

- (4) $\forall w \in W$, there exist constants $c, \delta > 0$ and integer $k < \infty$ such that

$$1 - c(p - w)^{2k} \geq f(p), \forall p \in [w - \delta, w + \delta]. \quad (\text{S12})$$

Lemma 1 [S3]. A function is constructible in quantum Bernoulli factory with $|\psi_p\rangle = \sqrt{p}|0\rangle + \sqrt{1-p}|1\rangle$ and a set of single-qubit unitary operations if and only if f satisfies SPB conditions.

Lemma 2 [S1]. Let $T(x_1, x_2, x_3) : \mathbb{R}^3 \rightarrow \mathbb{R}$ be a multivariate polynomial of x_1, x_2 and x_3 . Suppose $T(p, \sqrt{p}, \sqrt{1-p})$ is not a zero function. If $T(z, \sqrt{z}, \sqrt{1-z}) = 0$ for some $z \in [0, 1]$. Then there exist a real number δ , an integer k and a function $m(p)$ which is continuous in $[z - \delta, z + \delta]$, such that $T(p, \sqrt{p}, \sqrt{1-p}) = (p - z)^{\frac{1}{2}k} m(p)$ and $m(z) \neq 0$.

Proof. The proof of $\mathbb{Q} \subseteq \mathbb{Q}_1^1\mathbb{C}$ is similar to the proof of $\mathbb{Q}_1 \subseteq \mathbb{Q}_1^1\mathbb{C}$. The difference is concentrated in dealing with the continuity of f .

For the classical coins from \mathbb{Q}

$$q(p) = \frac{\sum_{j \in \mathbb{H}} |h_j(p)|^2}{\sum_{i \in \mathbb{B}} |h_i(p)|^2}, \quad (\text{S13})$$

where \mathbb{B} is the set of bases remained within the post selection of the measurement, and $\mathbb{H} \subseteq \mathbb{B}$ is the set of bases chosen for a head output. According to the main theorem, there exist a series of complex multivariate polynomials $R_i(x_1, x_2, x_3)$, such that

$$f(p) = \frac{\sum_{j \in \mathbb{H}} |R_j(p, \sqrt{p}, \sqrt{1-p})|^2}{\sum_{i \in \mathbb{B}} |R_i(p, \sqrt{p}, \sqrt{1-p})|^2}. \quad (\text{S14})$$

For arbitrary $f(p) \in \mathbb{Q}$, we prove that $f(p)$ satisfies the SPB conditions.

- (1) $f(p)$ is continuous. The only issue to consider about is that there might be some strange points that belong to both the zeros of the dominator and numerator. For example, we can construct a state

$$|\phi\rangle = (1-2p)|0\rangle + (1-2p)^2(1-3p)|1\rangle + (1-2p)(1-4p)^2|2\rangle + |3\rangle. \quad (\text{S15})$$

Note that this state is not normalized. Then we can obtain the classical function

$$s(p) = \frac{(1-2p)^2 + (1-2p)^4(1-3p)^2}{(1-2p)^2 + (1-2p)^4(1-3p)^2 + (1-2p)^2(1-4p)^4}. \quad (\text{S16})$$

via measurement if the outcome is $|0\rangle$ or $|1\rangle$ on condition of obtaining $|0\rangle$, $|1\rangle$ or $|2\rangle$. This function is continuous on $[0, 0.5) \cup (0.5, 1]$, and for other $p \in [0, 1]$, it behaves exactly the same with

$$s_e(p) = \frac{1 + (1-2p)^2(1-3p)^2}{1 + (1-2p)^2(1-3p)^2 + (1-4p)^4}. \quad (\text{S17})$$

Fortunately, we can handle this exception by using a small trick. Let $f_e(p)$ be the function after extracting factors involving the common zeros, so that there is no common zero between the numerator and dominator in $f_e(p)$ (such as $s_e(p)$ in equation (S17)). We denote the zeros of R_i as Z_i . It is easy to show that $f(p)$ is continuous in $[0, 1] - \bigcap_{i \in \mathbb{B}} Z_i$, and obviously, $f_e(p)$ is continuous in $[0, 1]$, and therefore $f_e(p)$ satisfies the SPB conditions, i.e. $f_e(p) \in \mathbb{Q}_1^1 \mathbb{C}$.

Since $f_e(p) : [0, 1] \rightarrow [0, 1]$ is constructible, it is of course that $f_e(p)$ is constructible when we limit the range of p , i.e. $f_e(p)$ is constructible for $p \in [0, 1] - \bigcap_{i \in \mathbb{B}} Z_i$. Therefore, we can simulate $f_e(p)$ for $p \in [0, 1] - \bigcap_{i \in \mathbb{B}} Z_i$, which is equivalent to simulate $f(p)$. In other words, we can extended $f(p)$ to $[0, 1]$, which is exactly $f_e(p)$. In this way, we can handle the continuity of the functions.

- (2) Both $Z = z_i : f(z_i) = 0$ and $W = w_i : f(w_i) = 1$ are finite sets. Because $R_i(x_1, x_2, x_3)$ are multivariate polynomials, so $|R_i(p, \sqrt{p}, \sqrt{1-p})|$ is bounded when $p \in [0, 1]$, and has finite zeros in $[0, 1]$. We can then find out that the set of Z is

$$Z = \left(\bigcap_{j \in \mathbb{H}} Z_j \cap [0, 1] \right) - \bigcap_{i \in \mathbb{B}} Z_i, \quad (\text{S18})$$

and obviously Z is finite. Similarly, $W = \left(\bigcap_{i \notin \mathbb{B}} Z_i \right) \cap [0, 1]$ is finite. In summary, both Z and W are finite. It is worth noting that at the breaking points of f (i.e. the joint set of all Z_i for $i \in \mathbb{B}$), the function f can be extended to be a continuous one with the inserted value given by equation (S17).

- (3) $\forall z \in Z$, there exist constants $c, \delta > 0$ and integer $k < \infty$ such that

$$c(p-z)^{2k} \leq f(p), \forall p \in [z-\delta, z+\delta]. \quad (\text{S19})$$

This can be easily checked using Lemma 2.

- (4) $\forall w \in W$, there exist constants $c, \delta > 0$ and integer $k < \infty$ such that

$$1 - c(p-w)^{2k} \geq f(p), \forall p \in [w-\delta, w+\delta]. \quad (\text{S20})$$

This just requires to have $1 - f(p) \geq c(p-w)^{2k}$. Note that w is then one of the zeros of $1 - f(p)$. Therefore the satisfiability of this condition can be similarly obtained through Lemma 2. ■

V. THE EQUALITY OF THE QC SETS

We provide an illustrative proof for this result, as shown in Fig. S1. We firstly show that $\text{QC} = \text{Q}_1^1\text{C}$. The quantum operations for type-3 QBF can reach a set denoted as Q , and with the above results, we know that $\text{Q} \subset \text{Q}_1^1\text{C}$. Therefore, we can just replace the quantum processor of type-3 QBF with a complete type-1 QBF. Then, because of that Q_1^1C is closed under the classical processing, the whole process is equivalent with a standard type-1 QBF, and we obtain the result that $\text{QC} = \text{Q}_1^1\text{C}$. Owing to the same reason, we also have that $\text{Q}^1\text{C} = \text{Q}_1^1\text{C}$.

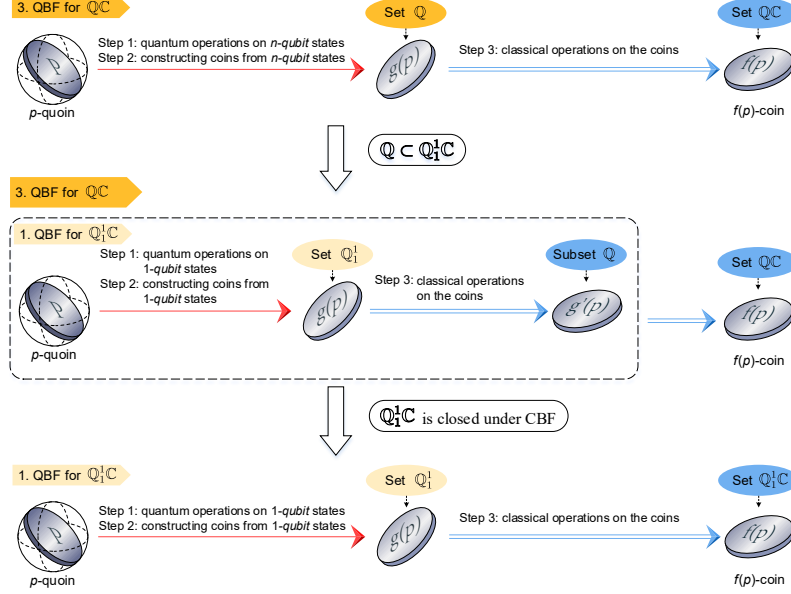


FIG. S1: The capability of QBFs in different types are the same.

VI. QBF PROTOCOLS FOR $g(p) = 4p(1-p)$ -COIN

Here we show that corresponding protocols in the view of framework of QBF for constructing function $g(p) = 4p(1-p)$. The classical function $g(p)$ is an important function, that servers as the core elements for many other functions. In ref. [S4], this function is experimentally constructed utilizing quantum coherence, and the results showed that quantum entanglement is not necessary for the construction. However, it has been experimentally shown that when utilizing quantum entanglement, the construction efficiency can be greatly enhanced, along with the reduction of resource consumption by two orders of magnitudes compared with the cases where only single-qubit operations are used.

The first protocol uses single-qubit operations, which has the following procedures.

- 1: [Quantum processing] generate a p -coin, which is done by directly measuring $|\psi_p\rangle$ in σ_z basis. Recall that a $f(p)$ -coin is a classical coin with probability $f(p)$ to output a head, and $1 - f(p)$ to output a tail;
- 2: [Quantum processing] generate a q -coin, where $q = \frac{1+2\sqrt{p(1-p)}}{2}$. This coin can be done by measuring $|\psi_p\rangle$ in D/A basis;
- 3: [Classical processing] construct an m -coin from a p -coin, where $m = 2p(1-p)$. This is a purely classical process by tossing the p -coin twice. Similarly, one can construct an n -coin where $n = 2q(1-q) = 1/2 - 2p(1-p)$;
- 4: [Classical processing] construct a s -coin from m -coin, where $s = m/(m+1)$, this procedure can be referred from ref. [S4] or section XI. Similarly, construct t -coin from n -coin, where $t = n/(n+1)$;
- 5: [Classical processing] construct a $g(p) = 4p(1-p)$ -coin from s -coin and t -coin. If the first toss is head, and the second toss is tail, then output head; if the first toss is tail and the second toss is head, then output tail; otherwise repeat this step.

The quantum state evolution in these procedures involves only single-qubit operation, which can be easily done on our photonic processor.

The second protocol for $g(p)$ -coin is finished in type-2 QBF, where arbitrary quantum operations can be applied for generating a single-qubit Bernoulli state, which is then measured to produce a classical coin for classical processing. In this protocol, the $g(p)$ -coin can be generated by solely quantum operations and no more classical processes are required, because there luckily exists a single-qubit state for the $g(p)$ -coin:

$$|\psi_g\rangle = \sqrt{4p(1-p)}|0\rangle + (2p-1)|1\rangle. \quad (\text{S21})$$

Measuring $|\psi_g\rangle$ in σ_z basis can directly obtain the $g(p)$ -coin. Assuring the existence of the corresponding Bernoulli state, we can then optimize the circuit that constructs $|\psi_g\rangle$, as shown in the following procedures.

- 1: [Quantum processing] Apply CNOT on $|\psi_p\rangle|\psi_p\rangle$, resulting in

$$|\psi_1\rangle = p|00\rangle + \sqrt{p(1-p)}|01\rangle + (1-p)|10\rangle + \sqrt{p(1-p)}|11\rangle. \quad (\text{S22})$$

- 2: [Quantum processing] Apply Hadamard operation on the first qubit to obtain

$$|\psi_2\rangle = \frac{1}{\sqrt{2}} \left(|00\rangle + 2\sqrt{p(1-p)}|01\rangle + (2p-1)|10\rangle \right). \quad (\text{S23})$$

- 3: [Quantum processing] Apply CNOT on $|\psi_2\rangle$, and post-selecting the second qubit in $|1\rangle$ basis will give

$$|\psi_g\rangle = \frac{1}{\sqrt{2}} \left(2\sqrt{p(1-p)}|0\rangle + (2p-1)|1\rangle \right). \quad (\text{S24})$$

- 4: [Quantum processing] Measure $|\psi_g\rangle$ will result in the target function.

The third protocol for $g(p)$ -coin is generating a multi-qubit Bernoulli states for probability measurement. The first two steps are the same with the second protocol, then we directly measure the probability from this 2-qubit state, and $g(p)$ is the probability of obtaining $|01\rangle$ on condition of obtaining $|01\rangle$ and $|10\rangle$

$$g(p) = \frac{|h_{|01\rangle}(p)|^2}{\sum_{i \in \{|01\rangle, |10\rangle\}} |h_i(p)|^2} = \frac{|2\sqrt{p(1-p)}|^2}{|2\sqrt{p(1-p)}|^2 + |(2p-1)|^2} = 4p(1-p). \quad (\text{S25})$$

Compared with the second protocol, this protocol requires less gate operations. The implementation of the post-selection together with the final measurement can be as complicated as the joint measurement, therefore we show that the protocol with multi-qubit Bernoulli states is the most efficient.

VII. THE STATE EVOLUTION IN THE EXPERIMENT

FIG. 2(e) in the main text shows the experimental proposal. The entangled photons are obtained through the type-I SPDC process. Before being injected into the two Sagnac interferometers, the photons are in the following state:

$$|\phi\rangle = \frac{1}{\sqrt{2}} (|00\rangle + |11\rangle), \quad (\text{S26})$$

where $|0\rangle$ and $|1\rangle$ represent the horizontal and vertical polarization respectively. Then each of the two photons goes into a Sagnac interferometer, which consists of a PBS/BS mixed crystal and three prisms. The PBS part of the cube converts the polarization-entanglement to the spatial entanglement, so that the state becomes:

$$|\phi_{\text{spatial}}\rangle = \frac{1}{\sqrt{2}} (|0\rangle_{1T}|0\rangle_{2T} + |1\rangle_{1R}|1\rangle_{2T}), \quad (\text{S27})$$

where $1T$, $2T$, $1R$ and $2R$ represent different spatial modes labelled in FIG. 2(e) (main text). Four groups of waveplates (including one HWP and one QWP), denoted by T_{1T} , T_{1R} , T_{2T} and T_{2R} (the labels are not marked in the

figure) are placed in each path. These waveplates work on the polarization of the four spacial modes, and prepare the states to

$$\begin{cases} T_{1H}|0\rangle = T_{1V}|1\rangle = |\varphi_1\rangle \\ T_{2H}|0\rangle = T_{2V}|1\rangle = |\varphi_2\rangle. \end{cases} \quad (\text{S28})$$

The initial state for the operations can be represented by

$$|\psi_{in}\rangle = \frac{1}{\sqrt{2}} (|\varphi_1\rangle_{1T}|\varphi_2\rangle_{2T} + |\varphi_1\rangle_{1R}|\varphi_2\rangle_{2T}). \quad (\text{S29})$$

The configurable parts in each spatial mode are then applied to the states. In our implementation, the elements placed in modes of $1T$ and $2T$ are fixed to be the projectors in horizontal and vertical polarizations respectively, with the elements in the other two spatial modes reconfigurable. These optical elements turn the state to

$$(M_0|\varphi_1\rangle_{1T} \otimes A|\varphi_2\rangle_{2T} + M_1|\varphi_1\rangle_{1R} \otimes B|\varphi_2\rangle_{2T}), \quad (\text{S30})$$

where M_0 and M_1 are the projectors to $|0\rangle$ and $|1\rangle$ respectively. The success probability of this step is $1/2$. A and B denote the two sets of configurable elements. After this operation, the spatial modes are mixed in the BS parts of the crystals. We post-select one of the ports of each crystal (where the probability amplitude is $\frac{1}{\sqrt{2}}$ for each photon), eliminating the path information, and the state becomes

$$\begin{aligned} & (M_0|\varphi_1\rangle \otimes A|\varphi_2\rangle + M_1|\varphi_1\rangle \otimes B|\varphi_2\rangle) \\ & = (M_0 \otimes A + M_1 \otimes B) |\varphi_1\rangle |\varphi_2\rangle, \end{aligned} \quad (\text{S31})$$

with success probability of $1/4$.

Finally, the configurable element C before the detector for the first qubit is applied on this state, and we obtained the final state

$$|\psi_o\rangle = (C \otimes I) (M_0 \otimes A + M_1 \otimes B) |\varphi_1\rangle |\varphi_2\rangle. \quad (\text{S32})$$

By configuring A , B , and C , we can realize different operations. It is worth noting that the reflection of the beam on the surfaces of prisms and the PBS/BS cube act as Pauli-Z gates, and can be compensated by a half-wave plate fixed at 0° .

A. State evolution within the multiply operation

In multiply operation, the circuit is shown in Fig. 2(c), where the Sagnac interferometers are configured to be a C-NOT gate. Specifically, the parts A and C are configured to identity, and B acts as a Pauli-X gate. For simplicity, the states in the following discussion are not necessarily normalized. The initial states are prepared to be

$$\begin{cases} |\varphi_1\rangle = h_1|0\rangle + |1\rangle \\ |\varphi_2\rangle = h_2|0\rangle + |1\rangle, \end{cases} \quad (\text{S33})$$

where h_1 and h_2 are the encoded parameters. Note that the states are not necessarily normalized. We can obtain a final state from equation (S32), that is

$$|\psi_{o1}\rangle = (I \otimes I) (M_0 \otimes I + M_1 \otimes X) |\varphi_1\rangle |\varphi_2\rangle. \quad (\text{S34})$$

Combine equation (S33) and equation (S34), the result state is

$$\begin{aligned} |\psi_{o1}\rangle &= (M_0 \otimes I + M_1 \otimes X) |\varphi_1\rangle |\varphi_2\rangle \\ &= h_1 h_2 |00\rangle + h_1 |01\rangle + |10\rangle + h_2 |11\rangle \end{aligned} \quad (\text{S35})$$

We then post-select the second qubit in $|0\rangle$ basis, and the result state collapses to

$$|\psi_m\rangle = h_1 h_2 |0\rangle + |1\rangle. \quad (\text{S36})$$

Interestingly, if we post-select the second qubit of $|\psi_o\rangle$ in $|1\rangle$ basis, we can implement a division operation instead, turning the outcome state to be $|\psi_d\rangle = \frac{h_1}{h_2} |0\rangle + |1\rangle$.

B. State evolution within the add operation

The circuit to implement the add operation is quite complicated, which is to implement a unitary denoted by B :

$$B = \begin{bmatrix} 1 & 0 & 0 & 0 \\ 0 & \frac{1}{\sqrt{2}} & -\frac{1}{\sqrt{2}} & 0 \\ 0 & \frac{1}{\sqrt{2}} & \frac{1}{\sqrt{2}} & 0 \\ 0 & 0 & 0 & 1 \end{bmatrix}. \quad (\text{S37})$$

The circuit requires 3 qubits and 5 control-operations.

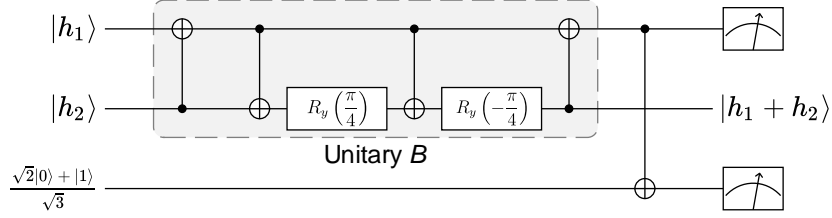


FIG. S2: Circuits for Add Operation By Implementing Unitary B

where the unitary B consists of 4 C-NOT gates and 2 single-qubit rotation gates. By applying unitary B on the first 2 qubits, we obtain

$$B|\psi_1\psi_2\rangle = h_1h_2|00\rangle + \frac{h_1 - h_2}{\sqrt{2}}|01\rangle + \frac{h_1 + h_2}{\sqrt{2}}|10\rangle + |11\rangle. \quad (\text{S38})$$

The post-selection of the first qubit in $|1\rangle$ basis makes the second qubit collapse into:

$$|\psi_{o2}\rangle = \frac{h_1 + h_2}{\sqrt{2}}|0\rangle + |1\rangle. \quad (\text{S39})$$

Then multiply $|\psi_{o2}\rangle$ with a constant state $(\sqrt{2}|0\rangle + |1\rangle)$ produces the final state:

$$|\psi_a\rangle = (h_1 + h_2)|0\rangle + |1\rangle. \quad (\text{S40})$$

We simplify the circuit, as shown in Fig. 2(d) in main text. Practically, the reversion on the first qubit is merged into the initial state preparation, that is, we prepare the initial state to be

$$\begin{cases} |\phi_1\rangle = \frac{1}{h_1}|0\rangle + |1\rangle \\ |\phi_2\rangle = h_2|0\rangle + |1\rangle. \end{cases} \quad (\text{S41})$$

The configurable elements are then reconfigured for the add operation. Specifically, A is configured as identity, B is the M_0X gate by using a half-waveplate and a polarizer, and C is the Hadamard gate. Combining with equation (S32), the output state before the post-selection is

$$\begin{aligned} |\psi_{o4}\rangle &= H \otimes I (M_0|\phi_1\rangle \otimes I|\phi_2\rangle + M_1|\phi_1\rangle \otimes M_0X|\phi_2\rangle) \\ &= (h_1 + h_2)|00\rangle + |01\rangle + (h_2 - h_1)|10\rangle + |11\rangle. \end{aligned} \quad (\text{S42})$$

Then, post-select the first qubit in $|0\rangle$ basis, and we will obtain the final state of $|\psi_a\rangle$ as shown in equation (S40). Similarly, if we post-select the first qubit in $|1\rangle$ basis, we can implement subtract operation instead.

C. Success probability of the operations

As discussed in the above section, the final state is obtained through several cascades of post-selections. From the representations of the final output state, we can find that the success probability is different according to different values of h_1 and h_2 .

The success probabilities for the multiply operation and add operation can be calculated by

$$\begin{cases} \Pr_m = \frac{|h_1|^2|h_2|^2 + 1}{8(|h_1|^2 + 1)(|h_2|^2 + 1)} \\ \Pr_a = \frac{|h_1 + h_2|^2 + 1}{16(|h_1|^2 + 1)(|h_2|^2 + 1)}. \end{cases} \quad (\text{S43})$$

It means that for some specific values of h_1 and h_2 , the success probability to obtain the result states become quite low, making it more difficult to evaluate the fidelity of the output state. The Probabilities of the two operations corresponding to the values of $|h_1|$ and $|h_2|$ are shown in Fig. S3. The maximum success probability for multiply operation reaches $\frac{1}{8}$ when $|h_1| = |h_2| = 0$ or $|h_1| = |h_2| = \infty$, corresponding to the cases where the initial state is $|HH\rangle$ or $|VV\rangle$. For add operation, the maximum success probability is reached at $\frac{1}{12}$, when $h_1 = h_2 = \pm \frac{\sqrt{2}}{2}$.

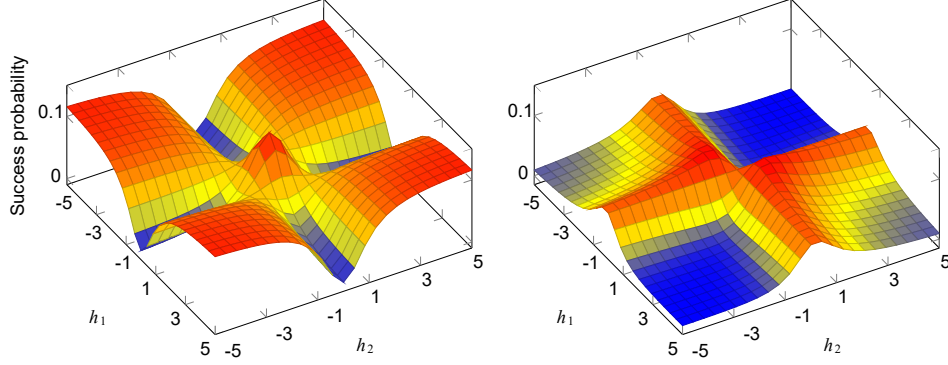


FIG. S3: Success probability with different real values of h_1 and h_2 , which is the same with the complex value cases. For the multiply operation (left), the probability would become quite low if one of h_1 or h_2 is 0 while the other holds a large norm; For the add operation (right), the case become that $h_1 + h_2 \sim 0$ while the norm of these two parameters are large.

VIII. DESIGNING QUANTUM ALGORITHM FOR THE EXAMPLE COIN WITH BASIC OPERATIONS

We start with some identical quoins $|p\rangle = \sqrt{\frac{p}{1-p}}|0\rangle + |1\rangle$. Note that the states are not necessarily normalized. Now we give the procedure for the example quoin $|f_q(p)\rangle = ((2p-1)|0\rangle + |1\rangle)$ in the main text.

1. Multiply two p -quoins, and obtain: $|\psi_1\rangle = \frac{p}{1-p}|0\rangle + |1\rangle$;
2. Add a constant quoin $\frac{-|0\rangle+|1\rangle}{\sqrt{2}}$ to $|\psi_1\rangle$, and obtain $|\psi_2\rangle = \frac{2p-1}{1-p}|0\rangle + |1\rangle$;
3. Add a constant quoin $\frac{|0\rangle+|1\rangle}{\sqrt{2}}$ to $|\psi_1\rangle$, and obtain $|\psi_3\rangle = \frac{1}{1-p}|0\rangle + |1\rangle$;
4. Reverse $|\psi_3\rangle$, and obtain $|\psi_4\rangle = (1-p)|0\rangle + |1\rangle$;
5. Multiply $|\psi_4\rangle$ with $|\psi_2\rangle$, and obtain the target quoin $|f_q(p)\rangle = (2p-1)|0\rangle + |1\rangle$.

It is easy to summarize this procedure in the form of circuit, as shown in Fig. S4.

The next step is of course to simplify this circuit. Since we found that the two add operations in step 2 and step 3 are perfectly symmetric, and therefore the two add operations together with the multiply operation in step 5 can be replaced by a single Hadamard gate. The circuit can be easily simplified to the form as shown in Fig. 5(a) in the main text. We can easily write the result state as

$$\begin{aligned} |\psi_{f_q(p)}\rangle &= ((X \cdot H) \otimes I)(M_0 \otimes I + M_1 \otimes X)|\psi_p\rangle|\psi_p\rangle \\ &= \frac{1}{\sqrt{2}(1-p)} ((2p-1)|0\rangle + |1\rangle) \otimes |0\rangle + \sqrt{\frac{2p}{1-p}}|11\rangle. \end{aligned} \quad (\text{S44})$$

By post-selecting the second qubit in the $|0\rangle$ basis, we can obtain the target state. The classical function $f_c(p) = \frac{(2p-1)^2}{1+(2p-1)^2}$ is obtained by directly measuring this state in σ_z basis.

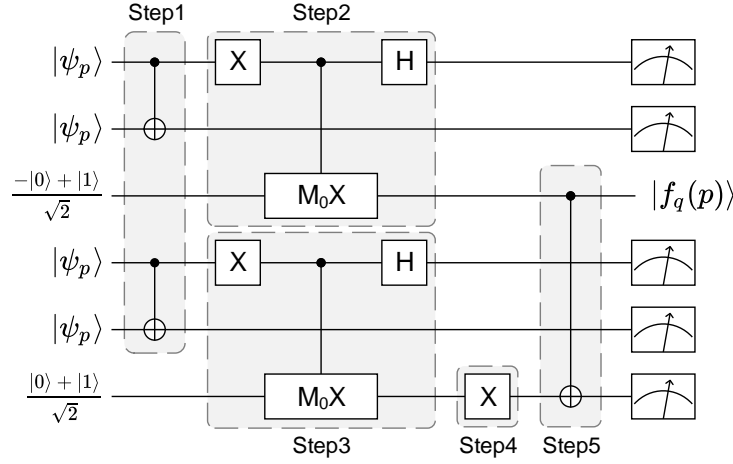


FIG. S4: Circuit for the example quoin using the three basic operations. This circuit requires totally 6 qubits and 5 2-qubit gates.

IX. EXPERIMENTAL PROPOSAL FOR $|p\rangle$

Besides the example of $|f_q(p)\rangle = (2p-1)|0\rangle + |1\rangle$, another important Bernoulli state is $|p\rangle = p|0\rangle + |1\rangle$. Though the corresponding classical coin is classically constructible, this state itself plays an important role in the construction of Bernoulli states [S1]. Note that the states are not necessarily normalized.

We start with the identical quoins $|\psi_p\rangle$. The procedure for the Bernoulli state $|p\rangle$ is similar with that for the example coin. By multiplying $|\psi_4\rangle$ with $|\psi_1\rangle$, we would directly obtain $|p\rangle$. However, the circuit for $|p\rangle$ is relatively harder to simplify, as shown in Fig. S5.

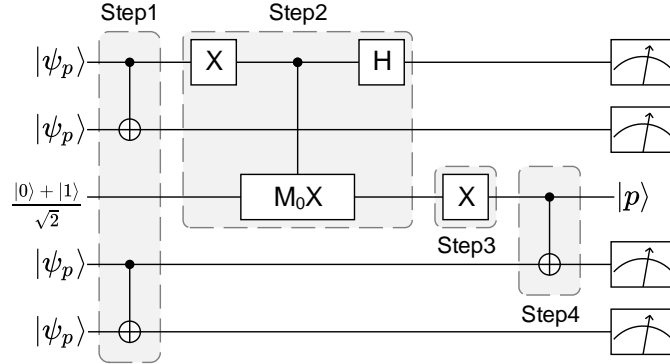


FIG. S5: Circuit for the example quoin using the three basic operations. This circuit requires totally 5 qubits and 4 2-qubit gates.

Fortunately, the photonic logic can be flexibly configured to generate this Bernoulli state. The photonic logic is first configured as a C-NOT operation, that is, A is configured to be identity, and B is configured to be X . Besides these configurations, several additional optical elements are placed in the control loop: a Hadamard gate is placed after the M_0 projector in the $1T$ route, and two projectors are placed after the M_1 projector in the $2T$ route to half the amplitude of the $|1\rangle$ part:

$$|\psi_{op}\rangle = (HM_0|\psi_p\rangle_{1T}) \otimes (HM_0|\psi_p\rangle_{2T}) + (M_1M_dM_1|\psi_p\rangle_{1R}) \otimes X|\psi_p\rangle_{2T} \quad (S45)$$

where M_d is the projector onto state $|+\rangle = \frac{1}{\sqrt{2}}(|0\rangle + |1\rangle)$. M_d with two M_1 operators can reduce the amplitude of $|1\rangle$ by a half. After having been mixed at the BS part of the mixed crystal, the state becomes:

$$|\psi_o\rangle = \frac{1}{2(1-p)} (p|0\rangle + |1\rangle) \otimes |0\rangle + \frac{p}{2(1-p)} |01\rangle + \left(\frac{p}{2(1-p)} + \frac{1}{2}\sqrt{\frac{p}{1-p}} \right) |11\rangle. \quad (S46)$$

Then if we obtain $|0\rangle$ when measuring the second qubit, the remaining qubit collapses into $|p\rangle$.

X. EVALUATION OF C-NOT GATE

We configure the photonic logic to be a C-NOT gate, and then use the method proposed in [S6] to evaluate the C-NOT gate. The process fidelity of the C-NOT gate can be evaluated through the measurement of two truth tables in complimentary basis and then calculate the classical fidelities of the two truth tables through

$$F_P = \frac{1}{N} \sum_{i=1}^N \Pr(f(i)|i) \quad (\text{S47})$$

where $\Pr(f(i)|i)$ denotes the probability to obtain the theoretical output $f(i)$ when the input i is given. We choose $\{|HH\rangle, |HV\rangle, |VH\rangle, |VV\rangle\}$ and $\{|DD\rangle, |DA\rangle, |AD\rangle, |AA\rangle\}$ as the bases for the fidelity evaluation, thus the classical fidelities can be calculated through

$$\begin{cases} F_{HV} = \frac{\Pr(HH|HH) + \Pr(HV|HV) + \Pr(VH|VV) + \Pr(VV|VH)}{4} \\ F_{DA} = \frac{\Pr(DD|DD) + \Pr(DA|AA) + \Pr(AD|AD) + \Pr(AA|DA)}{4} \end{cases} \quad (\text{S48})$$

The results of the two truth tables of the C-NOT gate in the form of coincidence counts are shown in TABLE SI.

TABLE SI: Truth tables of C-NOT gate. In both the tables, the first row represents the input basis and the first column represents the output basis. The coincidence counts are accumulated in 50 seconds.

	HH	HV	VH	VV
HH	2061	41	7	0
HV	41	1826	3	16
VH	14	15	39	1966
VV	15	7	2065	26

	DD	DA	AD	AA
DD	1580	5	105	12
DA	12	100	0	2060
AD	95	7	2132	6
AA	3	1939	13	117

By converting the coincidence counts into probability, as shown in TABLE SII, we can evaluate the classical fidelities of the two truth tables through

TABLE SII: Classical fidelity of the C-NOT gate. In both the truth tables, the first row represents the input basis and the first column represents the output basis. The data are sued for the bar graphes in Fig. 4 in main text

	HH	HV	VH	VV
HH	96.72%	2.17%	0.33%	0.00%
HV	1.92%	96.66%	0.14%	0.80%
VH	0.66%	0.79%	1.84%	97.91%
VV	0.70%	0.37%	97.68%	1.29%

	DD	DA	AD	AA
DD	93.49%	0.24%	4.67%	0.55%
DA	0.71%	4.88%	0.00%	93.85%
AD	5.62%	0.34%	94.76%	0.27%
AA	0.18%	94.54%	0.58%	5.33%

$$\begin{cases} F_{HV} = \frac{1}{4} (P_{HH \rightarrow HH} + P_{HV \rightarrow HV} + P_{VH \rightarrow VV} + P_{VV \rightarrow VH}) = 97.24\% \\ F_{DA} = \frac{1}{4} (P_{DD \rightarrow DD} + P_{DA \rightarrow AA} + P_{AD \rightarrow AD} + P_{AA \rightarrow DA}) = 94.16\%. \end{cases} \quad (\text{S49})$$

The process fidelity of the C-NOT gate can then be bounded by

$$F_{HV} + F_{DA} - 1 \leq F_P \leq \min(F_{HV}, F_{DA}), \quad (\text{S50})$$

and the fidelity over all input states through the average gate fidelity is calculated through

$$\bar{F} = \frac{N \cdot F_P + 1}{N + 1}, \quad (\text{S51})$$

where $N = 4$ for our 2 qubits system. The fidelities of the C-NOT gate then can be bounded as

$$\begin{cases} 91.40\% \leq F_P \leq 94.16\% \\ 93.12\% \leq \bar{F} \leq 95.33\%. \end{cases} \quad (\text{S52})$$

XI. QUANTUM ADVANTAGE THROUGH THE EXAMPLE COIN

The quantum advantage can be maximally illustrated in the example coin when $p = 0.5$. The photonic logic can generate $|f(p)\rangle$ with success probability

$$\text{Pr}_c = \frac{(2p-1)^2 + 1}{16} \quad (\text{S53})$$

which reaches the minimum value 0.0625 at $p = 0.5$. Thus averagely, it requires 16 $|\psi_p\rangle|\psi_p\rangle$ states to obtain one result coin. To identify the loss of transmission, we firstly prepare the state $|\psi_p\rangle|\psi_p\rangle$, and place no optical elements in the spatial modes, and accumulate the coincidence counts. Then we place the optical elements in, and accumulate the coincidence counts of the results state. By comparing the two results of coincidence counts, we found that around 2/5 photons would be lost during the transmission (mainly caused by the polarizers). Thus totally we need about 27 copies of $|\psi_p\rangle|\psi_p\rangle$ states, that is ~ 54 quinos for one result coin with $p = 0.5$.

Because of the experimental imperfection, the constructed function can be regarded as a truncated version $f_{ct}(p) = \max\left(\frac{(2p-1)^2}{1+(2p-1)^2}, \varepsilon\right)$, with $\varepsilon = 0.0424$, which is classically possible. To show the quantum advantage, we provide the classical procedure for constructing $f_{ct}(p)$, and compare the resource consumption of the procedures.

We first note that $f_c(p) = l(p)/(1+l(p))$ where $l(p) = (2p-1)^2$. Hence $l(p) = 1 - 4p(1-p)$ can be regarded as the reversed coin of $g(p) = 4p(1-p)$. Therefore the key procedure of constructing $f_c(p)$ is the construction of $g(p)$, which is studied in ref. [S4] and ref. [S5]. To suit the experimental imperfection, we can truncate $g(p)$ as $g_t(p) = \min(4p(1-p), 1 - 2\varepsilon_c)$, where $\varepsilon_c = 0.0221$. In this way, the number of coins required to construct a single $l(p)$ coin is [S4, S7]

$$n \approx \frac{-1}{\varepsilon_c^2} \ln\left(\frac{\varepsilon_c^2}{36}\right) \approx 2.285 \times 10^4, \quad (\text{S54})$$

Then we can construct the $f_c(p)$ -coin from $l(p)$ -coin, that by tossing $l(p)$ -coin twice, if the first toss is tail, then output tail; otherwise if the second toss is tail, output head; otherwise if both tosses are head, repeat this step. The averaged repeat time for this step is:

$$N = \sum_{i=1}^{\infty} i(1-l^2(p))(l^2(p))^{i-1} = \frac{1}{1-l^2(p)} \quad (\text{S55})$$

Since we have a truncation at $p = 0.5$, result in $l(0.5) = 0.0443$, and averagely it requires to toss $l(p)$ -coin for $2N$ times, where $2N \approx 2.190$. In total, the consumption of classical coins is $\sim 5.003 \times 10^4$. The quantum advantage is clearly shown here. This classical protocol is not optimal, but is enough for showing the quantum advantages.

XII. DETAILED DATA

We identified the quality of the output states by measuring its fidelity. Instead of doing a complete state tomography, we directly measure its fidelity because the theoretical output is already known, and we don't need other information contained in its density matrix. By measuring the counts of photons in the bases that parallel and orthogonal to the polarization of the theoretical state, we can evaluate the fidelity quickly. The data of the experiments are shown in TABLE [SIII~SV](#)

-
- [S1] Jiaqing Jiang, Jialin Zhang, and Xiaoming Sun. Quantum-to-quantum bernoulli factory problem. *Phys. Rev. A*, 97:032303, Mar 2018.
- [S2] M. S. Keane and George L. O'Brien. A bernoulli factory. *ACM Trans. Model. Comput. Simul.*, 4(2):213–219, April 1994.
- [S3] Howard Dale, David Jennings, and Terry Rudolph. Provable quantum advantage in randomness processing. *Nature Communications*, 6:8203 EP –, Sep 2015. Article.
- [S4] Xiao Yuan, Ke Liu, Yuan Xu, Weiting Wang, Yuwei Ma, Fang Zhang, Zhaopeng Yan, R. Vijay, Luyan Sun, and Xiongfeng Ma. Experimental quantum randomness processing using superconducting qubits. *Phys. Rev. Lett.*, 117:010502, Jun 2016.
- [S5] Raj B. Patel, Terry Rudolph, and Geoff J. Pryde. An experimental quantum bernoulli factory. *Science Advances*, 5(1), 2019.
- [S6] Holger F. Hofmann. Complementary classical fidelities as an efficient criterion for the evaluation of experimentally realized quantum operations. *Phys. Rev. Lett.*, 94:160504, Apr 2005.
- [S7] Șerban Nacu and Yuval Peres. Fast simulation of new coins from old. *Ann. Appl. Probab.*, 15(1A):93–115, 02 2005.

TABLE SIII: Results of the multiply operation. The initial state is prepared to be $(h_1|0\rangle + |1\rangle) \otimes (h_2|0\rangle + |1\rangle)$. The theoretical output state is $(h_1 h_2|0\rangle + |1\rangle)$. The labels correspond to the bars in Fig. 3 in main text. Terms denoted by “RxM” or “CxM” are random generated real or complex numbers. The coincidence counts are accumulated in 10 seconds, except for the “CxM” cases and the “LxM” cases where the time accumulated is about 1 minute. CC_{\parallel} is the coincidence counts obtained by setting the measurement basis parallel to the output state, and CC_{\perp} is the coincidence counts obtained by setting the measurement basis perpendicular to the output state.

Label	h_1	h_2	Initial State	$h_1 \cdot h_2$	Output State	CC_{\parallel}	CC_{\perp}	Fidelity
D1M	1.000	1.000	$ D\rangle D\rangle$	1.000	$ D\rangle$	514	20	96.255%
D2M	1.000	-1.000	$ D\rangle A\rangle$	-1.000	$ A\rangle$	455	26	94.595%
D3M	-1.000	1.000	$ A\rangle D\rangle$	-1.000	$ A\rangle$	636	23	96.510%
D4M	-1.000	-1.000	$ A\rangle A\rangle$	1.000	$ D\rangle$	562	23	96.068%
H1M	0.000	0.000	$ V\rangle V\rangle$	0.000	$ V\rangle$	893	1	99.888%
H2M	0.000	1.000	$ V\rangle D\rangle$	0.000	$ V\rangle$	513	4	99.226%
H3M	0.000	5.000	$ V\rangle(5 H\rangle + V\rangle)$	0.000	$ V\rangle$	38	7	84.444%
H4M	0.000	10.00	$ V\rangle(10 H\rangle + V\rangle)$	0.000	$ V\rangle$	36	8	81.818%
L1M	i	i	$ R\rangle R\rangle$	-1.000	$ A\rangle$	1074	49	95.637%
L2M	i	$-i$	$ R\rangle L\rangle$	1.000	$ D\rangle$	851	66	92.803%
L3M	$-i$	i	$ L\rangle R\rangle$	1.000	$ D\rangle$	878	51	94.510%
L4M	$-i$	$-i$	$ L\rangle L\rangle$	-1.000	$ A\rangle$	811	55	93.649%
R1M	0.663	0.682	Rand Real	0.452	Rand Real	579	18	96.985%
R2M	0.080	0.830	Rand Real	0.066	Rand Real	654	0	100.000%
R3M	0.700	0.900	Rand Real	0.630	Rand Real	490	20	96.078%
R4M	0.217	0.467	Rand Real	0.101	Rand Real	654	0	100.000%
R5M	0.024	0.719	Rand Real	0.017	Rand Real	535	0	100.000%
C1M	$-0.080 - 0.093i$	$-0.553 - 0.821i$	Rand Complex	$-0.031 + 0.117i$	Rand Complex	938	14	98.529%
C2M	$1.354 - 1.693i$	$2.455 - 1.979i$	Rand Complex	$-0.010 - 6.837i$	Rand Complex	1848	32	98.298%
C3M	$-0.385 - 0.934i$	$-0.050 - 0.155i$	Rand Complex	$-0.125 + 0.107i$	Rand Complex	818	32	96.235%
C4M	$-0.172 - 0.784i$	$-0.019 - 0.353i$	Rand Complex	$-0.273 + 0.075i$	Rand Complex	1018	32	96.952%
C5M	$0.876 + 0.182i$	$-0.184 - 0.893i$	Rand Complex	$-0.001 - 0.816i$	Rand Complex	1225	76	94.158%
C6M	$1.611 - 1.658i$	$1.119 - 1.065i$	Rand Complex	$0.036 - 3.576i$	Rand Complex	858	34	96.188%
C7M	$1.229 + 0.240i$	$-0.064 - 0.255i$	Rand Complex	$-0.017 - 0.329i$	Rand Complex	889	46	95.080%

TABLE SIV: Results of the add operation. The initial state is prepared to be $(h_1|0\rangle + |1\rangle) \otimes (h_2|0\rangle + |1\rangle)$. The theoretical output state is $((h_1 + h_2)|0\rangle + |1\rangle)$. “ ∞ ” in the table indicates the state of horizontal polarization. Terms denoted by “RxA” or “CxA” are random generated real or complex numbers for test. The coincidence counts are accumulated in about 10 seconds except for the “CxA” cases and “LxA” cases where the time accumulated is about 1 minute. CC_{\parallel} is the coincidence counts obtained by setting the measurement basis parallel to the output state, and CC_{\perp} is the coincidence counts obtained by setting the measurement basis perpendicular to the output state.

Label	h_1	h_2	Initial State	$h_1 + h_2$	Output State	CC_{\parallel}	CC_{\perp}	Fidelity
D1A	-1.000	1.000	$ A\rangle D\rangle$	0.000	$ V\rangle$	127	38	76.970%
D2A	1.000	1.000	$ D\rangle D\rangle$	2.000	$2 H\rangle + V\rangle$	291	6	97.980%
D3A	-1.000	-1.000	$ A\rangle A\rangle$	-2.000	$-2 H\rangle + V\rangle$	453	15	96.795%
H1A	0.000	0.000	$ V\rangle V\rangle$	0.000	$ V\rangle$	401	12	97.094%
H2A	∞	0.010	$ H\rangle(H\rangle + 100 V\rangle)$	∞	$ H\rangle$	160	6	96.386%
H3A	∞	0.100	$ H\rangle(H\rangle + 10 V\rangle)$	∞	$ H\rangle$	46	5	90.196%
H4A	∞	100.000	$ H\rangle(100 H\rangle + V\rangle)$	∞	$ H\rangle$	7	0	100.000%
H5A	0.010	∞	$(H\rangle + 100 V\rangle)$	∞	$ H\rangle$	315	0	100.000%
L1A	i	i	$ R\rangle R\rangle$	$2i$	$2i H\rangle + V\rangle$	741	15	98.016%
L2A	$-i$	$-i$	$ L\rangle L\rangle$	$-2i$	$-2i H\rangle + V\rangle$	707	23	96.849%
R1A	0.500	0.500	$(H\rangle + 2 V\rangle)(H\rangle + 2 V\rangle)$	1.000	$ D\rangle$	480	14	97.166%
R2A	-5.347	-3.168	Rand Real	-8.515	Rand Real	106	3	97.248%
R3A	-8.166	-0.945	Rand Real	-9.111	Rand Real	238	5	97.942%
R4A	-2.140	-1.881	Rand Real	-4.021	Rand Real	313	2	99.365%
R5A	-1.418	-6.335	Rand Real	-7.753	Rand Real	187	0	100.000%
R6A	-7.123	0.038	Rand Real	-7.085	Rand Real	241	6	97.571%
R7A	0.256	-1.125	Rand Real	-0.869	Rand Real	275	8	97.173%
C1A	$-0.400 + 2.288i$	$0.336 + 0.948i$	Rand Complex	$-0.065 + 3.237i$	Rand Complex	714	17	97.674%
C2A	$-0.693 + 2.360i$	$0.595 + 1.105i$	Rand Complex	$-0.096 + 3.465i$	Rand Complex	466	10	97.899%
C3A	$-0.148 + 1.188i$	$4.329 - 1.157i$	Rand Complex	$4.181 + 0.016i$	Rand Complex	283	1	99.648%
C4A	$0.853 + 1.024i$	$1.945 - 0.880i$	Rand Complex	$2.801 + 0.143i$	Rand Complex	312	12	96.296%
C5A	$0.184 + 0.035i$	$1.294 + 1.030i$	Rand Complex	$6.543 + 0.041i$	Rand Complex	502	35	93.482%
C6A	$-0.338 + 0.836i$	$0.309 + 0.981i$	Rand Complex	$-0.028 + 1.819i$	Rand Complex	831	20	97.650%
C7A	$0.794 - 0.024i$	$0.904 - 0.080i$	Rand Complex	$1.699 - 0.106i$	Rand Complex	972	20	97.984%
C8A	$0.136 + 0.090i$	$-0.119 - 0.911i$	Rand Complex	$0.018 - 0.823i$	Rand Complex	578	17	97.143%
C9A	$-0.928 + 0.905i$	$0.651 - 0.618i$	Rand Complex	$0.100 - 1.156i$	Rand Complex	285	17	94.371%

TABLE SV: Detailed data of the example $\frac{(2p-1)^2}{1+(2p-1)^2}$ coin. The initial state is prepared in $|\psi_p\rangle|\psi_p\rangle = (\sqrt{\frac{p}{1-p}}|0\rangle + |1\rangle) \otimes (\sqrt{\frac{p}{1-p}}|0\rangle + |1\rangle)$. We firstly construct a quoin represented by $|f_q(p)\rangle = (2p-1)|0\rangle + |1\rangle$, and measure its fidelity. By measuring this quoin in σ_z basis, we obtain the classical coin that presents head in probability of $\frac{(2p-1)^2}{1+(2p-1)^2}$. The coincidence counts are all accumulated in about 1 minute.

p	CC_{\parallel}	CC_{\perp}	Fidelity	CC_H	CC_V	$\text{Pr}_{\text{Theor.}}$	$\text{Pr}_{\text{Exp.}}$	Std.deviation
0.0	1086	3	99.725%	1589	1704	0.500	0.483	1.025×10^{-5}
0.1	809	7	99.142%	998	1538	0.390	0.394	1.408×10^{-5}
0.2	663	14	97.932%	594	1485	0.265	0.285	2.036×10^{-5}
0.3	515	15	97.170%	250	1294	0.138	0.161	4.111×10^{-5}
0.4	486	17	96.620%	118	1299	0.038	0.083	6.499×10^{-5}
0.5	388	14	96.517%	51	1151	0.000	0.042	1.165×10^{-4}
0.6	390	12	97.015%	112	1141	0.038	0.089	7.545×10^{-5}
0.7	423	7	98.372%	237	978	0.138	0.196	5.384×10^{-5}
0.8	505	9	98.249%	472	1049	0.265	0.310	3.161×10^{-5}
0.9	595	1	99.832%	776	1025	0.390	0.431	2.387×10^{-5}
1.0	751	1	99.987%	1109	1130	0.500	0.496	1.871×10^{-5}